Chemistry of Materials

Article

pubs.acs.org/cm

High-Throughput Screening of Extrinsic Point Defect Properties in Si and Ge: Database and Applications

Michael Sluydts,*[†,‡] Michael Pieters,[†,∥] Jan Vanhellemont,[§] Veronique Van Speybroeck,[†] and Stefaan Cottenier*[†,‡]

[†]Center for Molecular Modeling, Ghent University, 9052 Zwijnaarde, Belgium

[‡]Department of Electrical Energy, Metals, Mechanical Construction and Systems, Ghent University, 9052 Zwijnaarde, Belgium

[§]Department of Solid State Sciences, Ghent University, 9000 Ghent, Belgium

Supporting Information

ABSTRACT: Increased computational resources now make it possible to generate large data sets solely from first principles. Such "high-throughput" screening is employed to create a database of embedding enthalpies for extrinsic point defects and their vacancy complexes in Si and Ge for 73 impurities from H to Rn. Calculations are performed both at the PBE and HSE06 levels of theory. The data set is verified by comparison of the predicted lowest-enthalpy positions with experimental observations. The effect of temperature on the relative occupation of defect sites is estimated through configurational entropy. Potential applications are demonstrated by selecting optimal vacancy traps, directly relevant to industrial processes such as Czochralski growth as a means to suppress void formation.

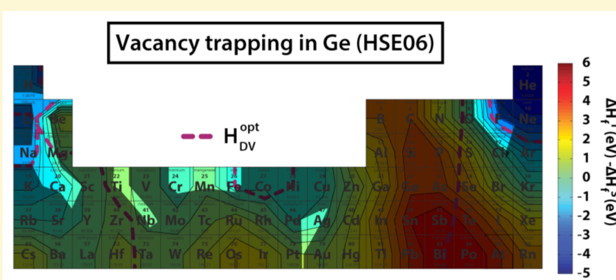

INTRODUCTION

Computational high-throughput screening allows sped-up discovery of (new) materials and their properties by using ab initio techniques to simulate a large set of candidates.[1] Ab initio methods allow a high degree of control over the studied systems and have now reached the level of maturity where simulations can be performed accurately without the need for human interaction.[2−4] The computational high-throughput approach enables better-focused experimentation by generation of reference data, discovery of trends, and identification of promising materials for desired applications. High-throughput screening has been previously used to discover new materials for photovoltaics, batteries, thermo- and piezoelectrics, catalysis, gas storage, and even superconductors.[5−11]

In this article we apply high-throughput screening to impurities in Si and Ge. While Si has been the focus of the semiconductor industry for the last 50 years, Ge has recently regained interest as a high-mobility substrate and is still commonly used in niche markets such as radiation detectors and space solar cells.[12−15] Impurities are essential to both materials, providing control over the semiconductor's properties during production and device operation. Knowledge of impurity properties in Ge is significantly less complete than for Si, and even for the latter only a subset of the periodic table has been studied.[12,16−30] Through high-throughput screening this knowledge can be considerably extended beyond what is currently experimentally known. In this way a complete and consistent data set can be provided for both materials and used to gain insights into future experimental and theoretical research as well as industrial applications. The latter is demonstrated by selecting candidate impurities for vacancy gettering in the Czochralski growth process.

METHOD

At the heart of our study lies a database of ab initio formation enthalpies of 876 extrinsic point defects and associated vacancy complexes in Si and Ge, making it the most extended set currently available. The entire database has been calculated both at the PBE level of theory and the higher HSE06 level.[31−33] The latter can require orders of magnitude more computational power but is able to correct various shortcomings in PBE such as the incorrectly vanishing band gap of Ge.[28,29,34−37] The availability of these data for a wide range of systems enables the direct quantification of the differences between them. This has not been previously possible, as earlier databases focused on a single level of theory equivalent to PBE. An example of such an earlier database is the one produced by Maeta and Sueoka[18] to study the diffusion barrier between substitutional and interstitial defect sites in Ge. This database contains formation enthalpies of three of the six positions presented here in both Si and Ge and for a large part of the periodic table. Despite their focus on Ge, only a generalized gradient approximation (GGA) method similar to PBE was studied. The database presented here adds 12 elements, the higher level of theory HSE06, and

Received: August 17, 2016
Revised: December 12, 2016
Published: December 12, 2016

 © 2016 American Chemical Society DOI: 10.1021/acs.chemmater.6b03368
Chem. Mater. 2017, 29, 975−984

three positions to enable the study of local vacancy interactions. The entire database, together with derived properties and CIF files for all 876 optimized geometries, can be found in the Supporting Information. Its potential use is demonstrated through two applications. First, the database is directly compared with experimental findings through the positions of known impurities. The second application illustrates how additional quantities can be derived from the database and used for impurity screening without performing any additional calculations. Specifically, an impurity is selected with the aim to improve single-crystal growth from a melt of Si or Ge by reducing void formation through vacancy gettering.

The defect formation enthalpy ΔH_f^D for a defect D is defined as

$$\Delta H_f^D = H_{sup}^D - n_H\mu_H - n_D\mu_D \quad (1)$$

in which H_{sup}^D is the enthalpy of a defect supercell, the chemical potentials μ_H and μ_D represent the enthalpies of the host and defect atoms in a reference structure, while n_H and n_D represent the numbers of these atoms present in the defect supercell. The elemental ground-state crystal structures are chosen as references for the impurity atoms. Because of the complexity of the ground-state crystal structures of S and Mn, simpler reference states were calculated and corrected using the known PBE energy differences between the two phases.[3]

Six positions are considered for each impurity, divided into three groups according to the number of host atoms in the cell. Each group contains two distinct nearest-neighbor environments between which migration is possible, as shown in Figure 1.

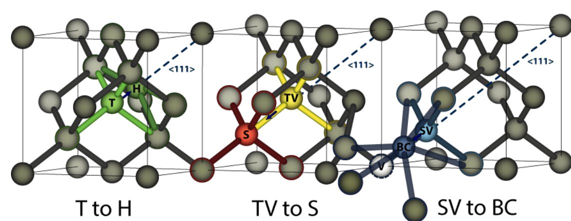

Figure 1. Positions and migration pathways for the three pairs discussed in the text.

The basis of the first group is an untouched host lattice, in which the impurity occupies an interstitial site with either tetrahedral (T) or hexagonal (H) coordination. The second group is created from a single vacancy, resulting in a substitutional (S) position when the vacancy is filled by the impurity or a tetrahedral−vacancy pair (TV) when the vacancy is created next to a T interstitial. The final group is based on a divacancy, either a substitutional−vacancy pair (SV) or a bond-centered (BC) position with the impurity placed in the center of the divacancy. The total energies in the database show that migration typically occurs from lower to higher coordination (T to H, TV to S, and SV to BC). In the case of the TV site, migration is often partial, with the impurity settling in a trifold planar configuration coordinated by the three common neighbors of the S and TV sites. This site is termed an off-center substitutional site (S_{off}). Symmetry conservation is imposed on all of the calculations, explicitly forbidding the appearance of configurations with broken symmetry. In particular for the lighter elements, symmetry breaking could sometimes lower the enthalpy further.

Each of the six positions has been calculated for 73 different impurity elements. Including reference states, this results in over 1000 structures to optimize. Screening at this scale requires a careful choice of method, where the computational cost must be weighed against the accuracy required. In our case, the accuracy of the formation enthalpy must be sufficient to observe trends throughout the periodic table. With this in mind, periodic PBE density functional theory (DFT) was chosen as main calculation method when geometric relaxations were performed. Final formation enthalpies were also evaluated using the HSE06 hybrid functional.

In all cases, global charge neutrality is conserved within the simulated cell. Atoms can acquire an effective charge through local polarization of the charge density, but it cannot be guaranteed that the experimental oxidation state will be obtained in all cases. The database is defined by the positions studied, the level of theory chosen, and the charge states simulated and represents a well-defined search space. These choices are acceptable and even essential to the paradigm of high-throughput screening. The resulting database can be expanded in follow-up studies. Typical strategies are the selection of isolated cases to perform high-precision calculations of either the same or novel properties or expanding the existing database with additional high-throughput studies of different charge states, configurations, and properties at a similar level of theory.

■ RESULTS

Lowest-Enthalpy Positions. Experimentally observed impurity positions are shown in Figure 2a,b, with the corresponding PBE-calculated lowest-enthalpy positions in Figure 2c,d and the HSE06 equivalents in Figure 2e,f. White areas in the experimental figures mark elements for which no position information is available. In these cases the ab initio results may provide information complementary to the experimental results. Discussion will commence with the PBE results, followed by an elaboration of the modifications caused by the Hartree−Fock (HF) contribution. A large part of the periodic table, both in Si and Ge, prefers a substitutional position. Since this typically minimizes distortions of the lattice, this result is not surprising. A major difference between Si and Ge is the preference of the 3d transition metals for interstitial sites in Si, typically T. For both materials, interstitial preference is also present for small alkali metals and noble gases, both of which interact weakly with the lattice, providing insufficient compensation for broken bonds of the host crystal. This can also be seen in the experimental results, which closely match the PBE positions. For larger atoms, the interstitial-induced lattice strain becomes too large, making it enthalpically favorable to create and fill a vacancy. For Si, which has higher bond strengths and less diffuse and polarizable valence orbitals, this is typically an S_{off} position, whereas in the case of very large atoms the S and T sites are simultaneously occupied. In the case of Ge, an SV complex is more beneficial because of the lower enthalpic cost of creating vacancies. Some of the smaller atoms also prefer the S_{off} position, which typically remains close to the trifold planar configuration, sometimes distorted toward the substitutional position. In Si these are O, Cl, and Br, while in Ge they consist of Cl and Kr. The S_{off} site offers the smallest possible bond lengths within our set, and minimizing bond lengths is exactly what these impurities attempt to do. This observation suggests that in these cases lesser-coordinated, symmetry-broken sites might lower the enthalpy even further. Such sites are indeed experimentally observed for O and N.[19,38] When the latter lower-symmetry sites are explicitly simulated, both elements strongly prefer an interstitial site,

DOI: 10.1021/acs.chemmater.6b03368
Chem. Mater. 2017, 29, 975−984

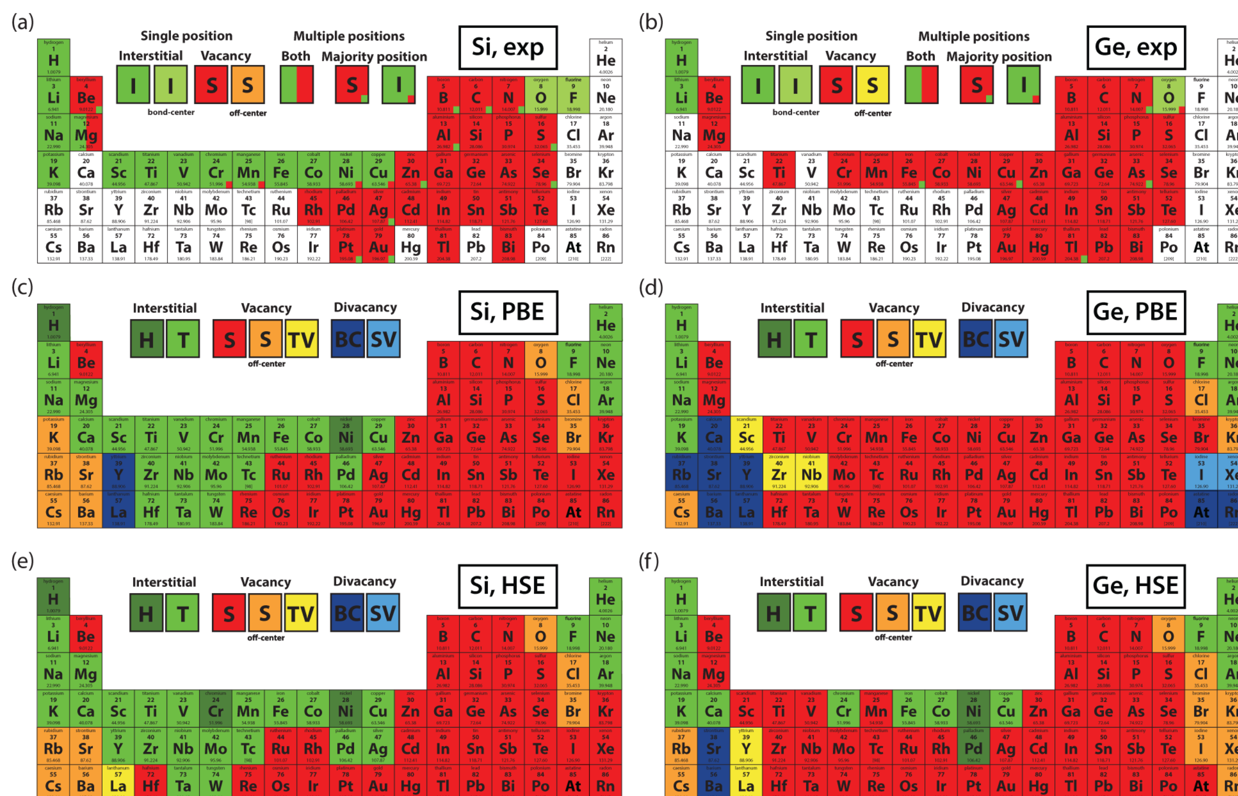

Figure 2. Most common experimental impurity positions for (a) Si[16−19] and (b) Ge,[12,16−23] mostly taken from refs 16 and 17, which represent data collected in the Landolt-Börnstein series, compiled from >50 experimental papers. These are compared to the lowest-enthalpy DFT predictions using PBE for (c) Si and (d) Ge and using HSE06 for (e) Si and (f) Ge. The description of the experimental positions is limited to interstitial (I) and substitutional (S), while the DFT predictions cover the six positions shown in Figure 1.

twofold-coordinated for O and trifold-coordinated for N, as well as a distorted substitutional site. Maeta and Sueoka examined the twofold-coordinated site for larger elements also but found that it quickly becomes enthalpically unfavorable.[18] The remaining TV positions in Ge consist of transition metals, which are capable of increased interactions through their incomplete d shells. Finally, the lanthanides, and in Ge also the alkaline-earth metals, prefer the bond-centered position. These elements are both sufficiently large and have sufficient numbers of free valence electrons to undergo bonding with the six nearest neighbors in the BC site. Results for Lu, which have been calculated but are not shown in the figures, suggest that the entire lanthanide series will remain in this position for Ge. In Si, lanthanides will switch from T to BC at some point for the same reason as the 3d transition metals.

When comparing these results with those obtained using the HSE06 functional, one sees that the site-specific regions are maintained but that the boundaries between the regions have shifted. Systematic trends are visible, most notably for the BC and SV positions, which are much less favored by HSE06. Additionally, an interstitial region appears for small transition metals in the case of Ge. These changes can be largely attributed to a single cause, namely, the increase in the formation enthalpy of the vacancy (~1 eV), implying increased cohesion of the crystal. This was previously observed by Śpiewak and co-workers, and the HSE06 values were found to correspond much more closely to experiment.[34,35] This effect delays the onset of vacancy creation as a means of lattice strain reduction. However, experimentally the interstitial region for the transition metals is not observed. This discrepancy is most likely a precision issue. A change in lowest-enthalpy positions implies a crossing of the relevant enthalpy curves. The nature of the crossing, combined with the lowered precision for HSE06 calculations, may cause an interchange of positions in some cases and subsequently a shift in region boundary. In the interstitial region of the transition metals, the interstitial and substitutional curves run roughly parallel, which increases their susceptibility to this behavior. Nonetheless, contributions by phenomena not considered in the model used may provide alternative explanations. Small energy shifts may be induced by symmetry breaking, for instance due to Jahn−Teller distortions, which could explain small shifts for the transition metals. This study also supposes overall charge neutrality, a condition that experimentally may not be necessarily met. However, the overall agreement between the calculated and observed positions suggests that the geometric effects of charged impurities may be limited. Especially outside of the transition metal region this can be expected, where the enthalpy difference between interstitial and substitutional positions is often predominantly determined by lattice strain. The resultant enthalpy difference between the subsitutional and interstitial positions is several electron volts in many cases and would require a very large change in the formation enthalpy of the charged defects to change the order of the positions. If a charged defect forms the ground state, the formation enthalpy is still expected to be positive, as most impurities will not spontaneously occur. This implies that the enthalpy curves are again compressed, in contrast to the spread caused by HSE06 as a consequence of the increased cost of vacancy formation. Similarly, a charged vacancy could be lower in energy and alter

DOI: 10.1021/acs.chemmater.6b03368
Chem. Mater. 2017, 29, 975−984

the energy and charge state of the complexes. For instance, negatively charged vacancies occur under n-type conditions both in Si and Ge.[24,28]

The enthalpy curves, grouped by period, can be found in the Supporting Information.

Relative Occupancies at the Melting Temperature. The lowest-enthalpy positions discussed in the previous section represent the sites relevant at 0 K. When temperature is introduced, rather than a single position, a distribution of sites will be occupied. This distribution will be determined not only by the relative enthalpy differences between these sites but also by their entropies. Taking this into account requires switching from the formation enthalpy ΔH_f to the formation Gibbs free energy ΔG_f (per 2 × 2 × 2 supercell):

$$\Delta G_f = \Delta H_f - T\Delta S_f \tag{2}$$

where ΔS_f is the formation entropy and T is the relevant temperature. Entropic contributions can be separated into various components: configurational, vibrational, electronic, and magnetic. In the dilute limit the configurational entropy increases because of the higher availability of impurity sites; however, the vibrational entropy remains approximately constant because the interactions with the lattice can be considered local. This causes the configurational entropy to become more important in the dilute limit.[37] As a result, calculating the computationally expensive vibrational entropy can be safely avoided. The electronic contribution is typically negligible even at high temperature, and the studied systems contain only a single defect, which in most cases is not magnetic.

The configurational entropy per 2 × 2 × 2 supercell can be deduced from the number of associated microstates W through the Boltzmann expression for entropy:

$$S = k_B \ln W \tag{3}$$

where k_B is Boltzmann's constant. The number of microstates that can be constructed for a given defect position using n defects in a cell of N atoms with g available configurations per host atom is given by

$$W = \binom{gN}{n} = \frac{(gN)!}{(gN-n)!n!} \tag{4}$$

This enables the construction of the configurational entropy for each defect. The resulting ΔG_f can then be used to construct a Boltzmann distribution that will determine the relative occupation P_D of each defect:

$$P_D = \frac{e^{-\Delta G_f^D/k_BT}}{Z} \quad \text{with} \quad Z = \sum_{D}^{\text{all sites}} e^{-\Delta G_f^D/k_BT} \tag{5}$$

where D is the considered impurity configuration and Z is the canonical partition function. Relevant values per site can be found in Table 1.[37]

The entropy is determined by the multiplicity g of the defect site per lattice atom. For the S and T sites, only one defect can be created per lattice site, resulting in $g = 1$. Vacancy complexes are created by removing an atom from a defect site's nearest-neighbor shell. Since only one of the four atoms in the shell is removed, the complexes have a multiplicity of $g = 4$. H and BC can be seen as higher-symmetry positions between two neighboring T and SV sites, respectively, resulting in multiplicities halved with respect to those of their sites of origin. It should be noted that in the case of vacancy complexes only the considered directly interacting vacancy pairs are included, while in reality configurations also exist where the vacancy is found at varying distances in further nearest-neighbor shells. However, these are typically less enthalpically favored, as vacancy pairs are often created to locally reduce lattice strain, often with occupancy of the vacancy by the impurity as a consequence.

Table 1. Quantities Used in the Calculation of the Configurational Entropy of a Single Defect (n = 1) in a 64-Atom Host Cell (N = 64) at the Melting Temperature (1687 K for Si and 1211 K for Ge)

	T	H	S	TV	BC	SV
g	1	0.5	1	4	2	4
W	64	32	64	256	128	256
$T_{melt,Si}S$ (eV)	0.50	0.50	0.60	0.80	0.70	0.80
$T_{melt,Ge}S$ (eV)	0.43	0.36	0.43	0.57	0.5	0.57

The impact of the configurational entropy contribution can become very sizable at the melting temperature. Because of the normalization procedure, however, the relative occupations are determined only by Gibbs free energy differences and, consequently, differences in entropy. This also has the positive side effect that the relative occupation does not change with respect to concentration. These relative occupations at the melting temperature are depicted in Figure 3. Each element's box is colored proportionally to each site's occupation.

Even at the melting temperature the overall occupancy picture has changed very little. When comparing the PBE results with their 0 K counterparts, one does see that many of the T interstitial positions in Si also obtain a minority S occupation. The S_{off}/TV regions also clearly expand because they are entropically favored, as can be seen for the noble gases (S to S_{off}) and also for Y and La (BC to TV). This same preference for asymmetry is visible in Ge, where TV and S_{off} become favorable for transition metals and chalcogens while the lower-symmetry SV position becomes more prominent for larger elements. The behavior for HSE06 is very similar, but with position ratios sometimes differing between, for instance, S and T sites. As previously discussed, vacancies undergo an energetic penalty in HSE06, which is the reason why SV/BC positions are very rare at thermodynamic equilibrium while interstitials become more prominent. The larger spread in formation energy also causes the TV region in the transition metals to be less extended. It should be noted that the lattice model used here represents a simplification of the true situation, where impurities may diffuse in three-dimensional continuous space. Here, many more local minima can be present that may be highly similar to the positions studied here or represent additional sites. If that happens, the configurational entropy may greatly increase, and the balance between different positions could shift. Such effects have, for instance, been previously observed in the clustering of point defects by Kapur et al.[39]

Vacancy Trapping at 0 K. The second property of interest is the vacancy trapping enthalpy. During single-crystal growth from a melt, vacancies can agglomerate and form voids, leading to problems with epitaxy and gate oxide integrity, among others. One way to prevent this without affecting the crystal electrical properties is trapping of vacancies by impurities.[28] These impurities may be electrically active or not, depending on the requirements of the application. Trapping occurs when it becomes enthalpically beneficial for the vacancy to reside near the impurity. Since the diffusivities of substitutional impurities

DOI: 10.1021/acs.chemmater.6b03368
Chem. Mater. 2017, 29, 975−984

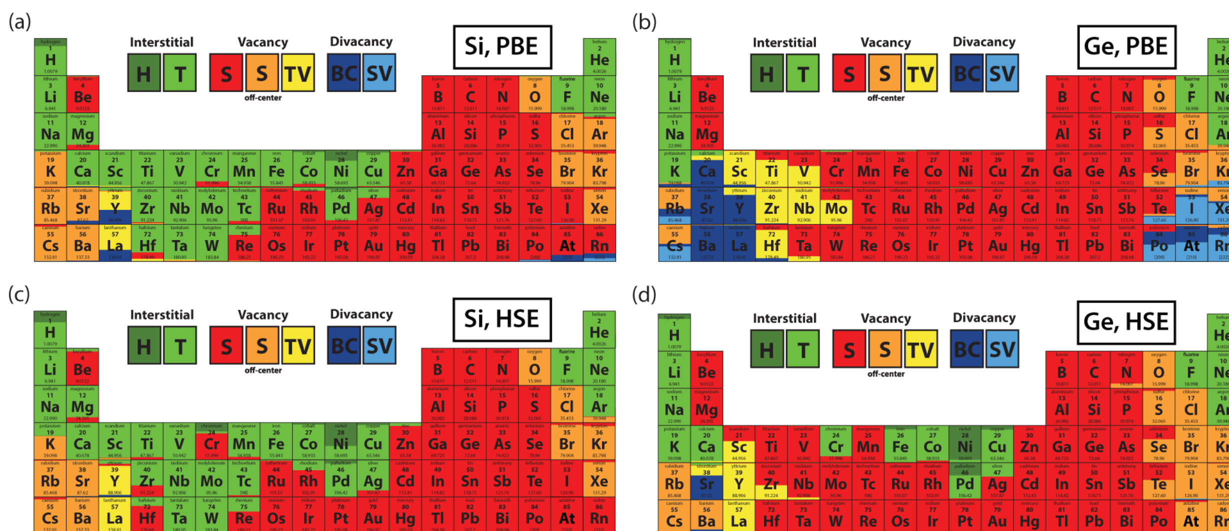

Figure 3. Relative occupancies at the melting temperature calculated using the PBE functional for (a) Si and (b) Ge and the HSE06 functional for (c) Si and (d) Ge. Vertical ordering or colored regions correspond to horizontal ordering within the legend.

are typically much lower than that of a vacancy, a trapped vacancy is less likely to agglomerate.[17,40,41]

This can be quantified through the trapping enthalpy H_{SV} or H_{TV} (denoted as H_{DV}, with D = S or T), which expresses the energy cost of creating a trapped vacancy out of a defect and a vacancy (negative values mean that energy is being released):

$$H_{DV} = \Delta H_f^{DV} - \Delta H_f^{D} - \Delta H_f^{V} \quad (6)$$

where each ΔH_f is the formation enthalpy of the relevant defect. Each of them is available in the database, including the vacancy formation enthalpy ΔH_f^V. The latter is included as the SV defect with Si or Ge as the "impurity"; in PBE this corresponds to 3.6 eV for Si and 2.5 eV for Ge, while for HSE06 values of 4.4 eV for Si and 3.5 eV for Ge are found. This is in good agreement with known ab initio and experimental results.[34,35,42]

The next step is to create a set of criteria that reduce the full screening set to a subset of potentially interesting impurities. The actual criteria may vary depending on the experimental situation and in an industrial context may even include economic constraints.[43] As an illustration of the method, the following criteria were used:

- It should be favorable to form the complex from the isolated vacancy and the free trap. Additionally, to prevent void formation, trapping by impurities should be more favorable than trapping by vacancies:

  $$H_{DV} < \min(0, H_{VV}) \quad (7)$$

  The vacancy–vacancy trapping enthalpies are H_{VV} = −1.8 eV in Si and −0.8 eV in Ge at the PBE level and −2.2 eV in Si and −1.5 eV in Ge at the HSE06 level.
- Sufficient free traps should be present compared with vacancies and the complex—the latter as buffer for changes in vacancy concentration:

  $$\Delta H_f^D < \min(\Delta H_f^V, \Delta H_f^{DV}) \quad (8)$$

  Together with eq 6, this requirement leads to the following condition:

  $$H_{DV} > -\Delta H_f^V \quad (9)$$

  The latter expresses that the energy released by merging a defect and a vacancy should not be larger than the energy needed to create a vacancy. If this were to happen, then any trapping event would generate more vacancies, and the trap would not be effective.

Equations 7 and 9 lead to upper and lower bounds for H_{DV}: $-\Delta H_f^V < H_{DV} < H_{VV}$. Choosing an element for which H_{DV} is maximally negative (i.e., close to the lower bound, $H_{DV} = -\Delta H_f^V$) implies by eq 7 that the condition expressed by eq 9 is only barely met: the number of free traps is not abundant. On the other hand, choosing an element for which H_{DV} is close to the upper bound ($H_{DV} = H_{VV}$) implies that the trapping strength is small: vacancies can leave the trap to form vacancy clusters without penalty.

The best candidates are the ones with an optimal trade-off between the conflicting requirements of a large equilibrium concentration of free traps and a large trapping strength. For this a simple exponential average is used, since both the initial vacancy concentrations and diffusion coefficients vary exponentially within the interval:

$$H_{DV}^{opt} = \ln\left(\frac{e^{H_{VV}} + e^{-\Delta H_f^V}}{2}\right) \quad (10)$$

This yields the following intervals and optimal values for PBE:

- for Si: −3.6 eV < H_{DV} < −1.8 eV; H_{DV}^{opt} = −2.3 eV; ΔH_f^D < 3.6 eV
- for Ge: −2.5 eV < H_{DV} < −0.8 eV; H_{DV}^{opt} = −1.4 eV; ΔH_f^D < 2.5 eV

The intervals and optimal values for HSE06 are:

- for Si: −4.4 eV < H_{DV} < −2.2 eV; H_{DV}^{opt} = −2.8 eV; ΔH_f^D < 4.4 eV
- for Ge: −3.5 eV < H_{DV} < −1.5 eV; H_{DV}^{opt} = −2.0 eV; ΔH_f^D < 3.5 eV

The vacancy trapping data for Si are graphically presented in Figure 4. For the substitutional impurities, the major elimination of candidates is caused by the criterion for H_{SV}. The limitation on ΔH_f^S leads to the additional elimination of most alkalis, noble gases, and W. Optimal substitutional traps are the light elements Li, Mg, F, and Cl as well as the transition metals

DOI: 10.1021/acs.chemmater.6b03368
Chem. Mater. 2017, 29, 975−984

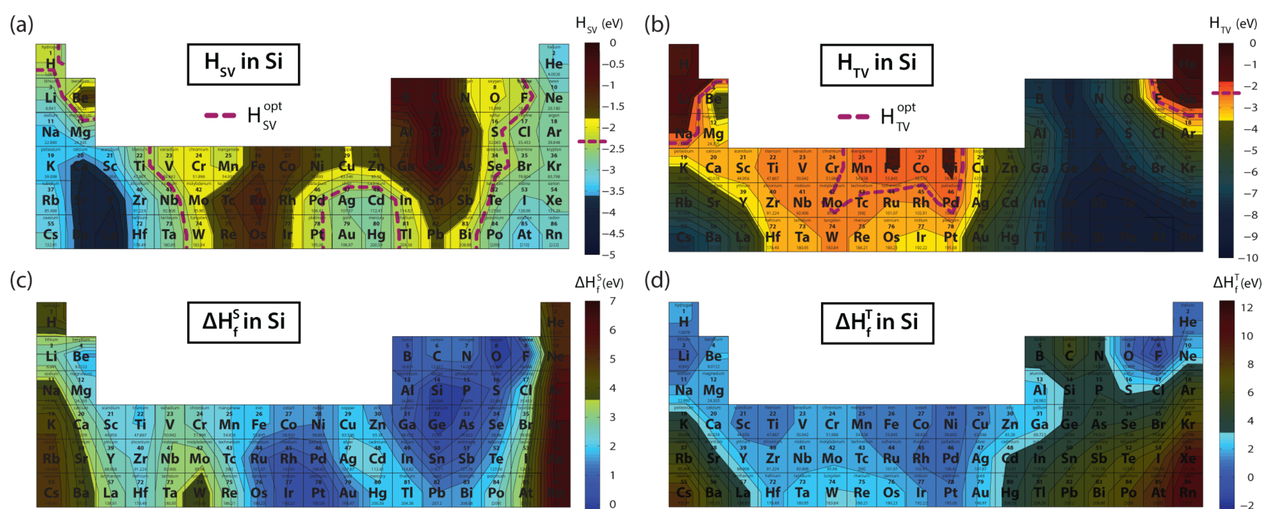

Figure 4. Optimal H_{DV} regions for (a) S and (b) T traps and formation enthalpies of the free (c) S and (d) T traps for Si. Contours were created by interpolating enthalpic data points at the center of each element's box. Dashed purple lines represent H_{DV}^{opt}, while areas outside of the optimal interval have been darkened.

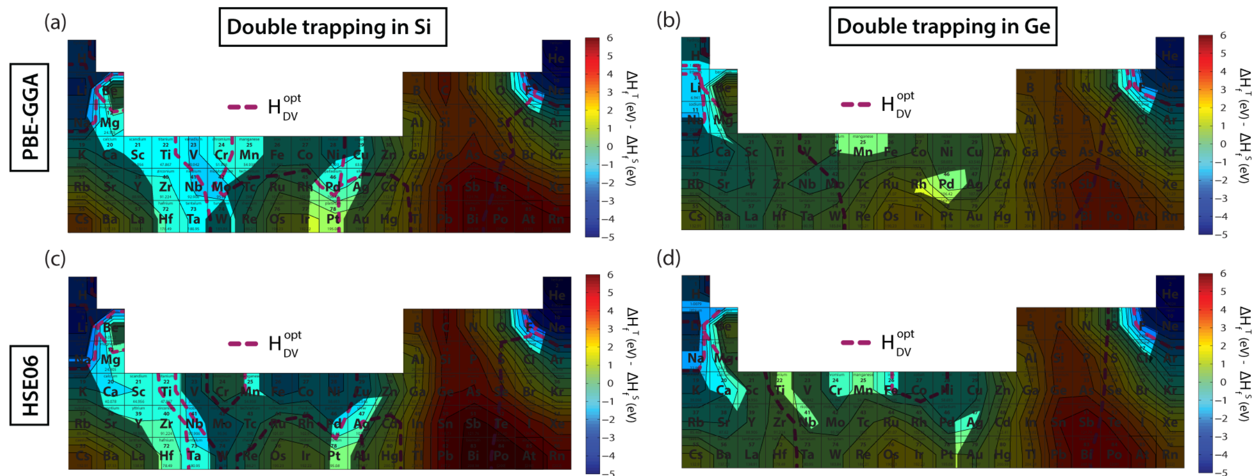

Figure 5. Optimal double-trapping regions with the PBE functional for (a) Si and (b) Ge and with the HSE06 functional for (c) Si and (d) Ge. Here the contours represent $\Delta H_f^T - \Delta H_f^S$, and all areas excluded in Figure 4 have been darkened. Double trapping is most likely when the first free trap is more prevalent, i.e., where $\Delta H_f^T - \Delta H_f^S$ is negative.

Ti, V, Nb, W, Pt, Pd−In, and Tl and the p-block elements S, Se, Te, and Bi. For the T interstitial impurities, the limitation on H_{TV} leaves only most transition metals, some light (earth)alkalis, and F−Ar. Ar is the only element that is additionally eliminated on the basis of the ΔH_f^T criterion. The surviving optimal interstitial traps are the light elements Na and Be (both only marginally optimal) and the transition metals Cr, Mo−Pd, and perhaps Ni, as well as F and to a lesser extent also Ne−Ar. When the experimental symmetry-broken defect configurations are explicitly simulated, a significantly lower formation enthalpy ΔH_f^D is found, which may greatly increase the number of free traps in this case and outweigh their suboptimal trapping behavior. However, the explicit trapping enthalpy for these positions was not calculated. It is also possible that more complex configurations come into play, including the mutual interaction of O and N impurities.[44]

Looking at the cross sections of the H_{DV}^{opt} lines and the overlap of the allowed intervals enables a search for possible double traps. This is illustrated for Si in Figure 5a, where all four allowed PBE intervals from Figure 4 are combined. The combined PBE results for Ge are shown in Figure 5b, while the HSE06 equivalents for Si and Ge can be found in Figure 5c,d, respectively. In each case, the enthalpy contours now represent $\Delta H_f^T - \Delta H_f^S$. Elements for which the latter value is negative (and therefore fall simultaneously in both allowed intervals) that are also near a crossing of the H_{SV}^{opt} and H_{TV}^{opt} lines are promising candidates for double traps. With PBE these are Li−Be, Nb−Mo, Pd, and F for Si. For Ge, only Li−Be and F survive, but the only remaining transition metals, Pd and Mn, represent a similar region to the one found for Si. In the case of HSE06, minor changes take place. The double-trapping regions contract for Si and slightly expand for Ge, with minor shifts of the optimal-value curves occurring in both cases. The reason for this difference in behavior is actually a flat trapping enthalpy surface in the V−Cr region. This causes these elements to be excluded for Si while there is actually an expansion of the optimal region toward the bottom-left of the periodic table, a consequence of increased enthalpy differences between positions in HSE06. Despite these changes, however, the optimal choices largely stay the same. This is the case because the

DOI: 10.1021/acs.chemmater.6b03368
Chem. Mater. 2017, 29, 975−984

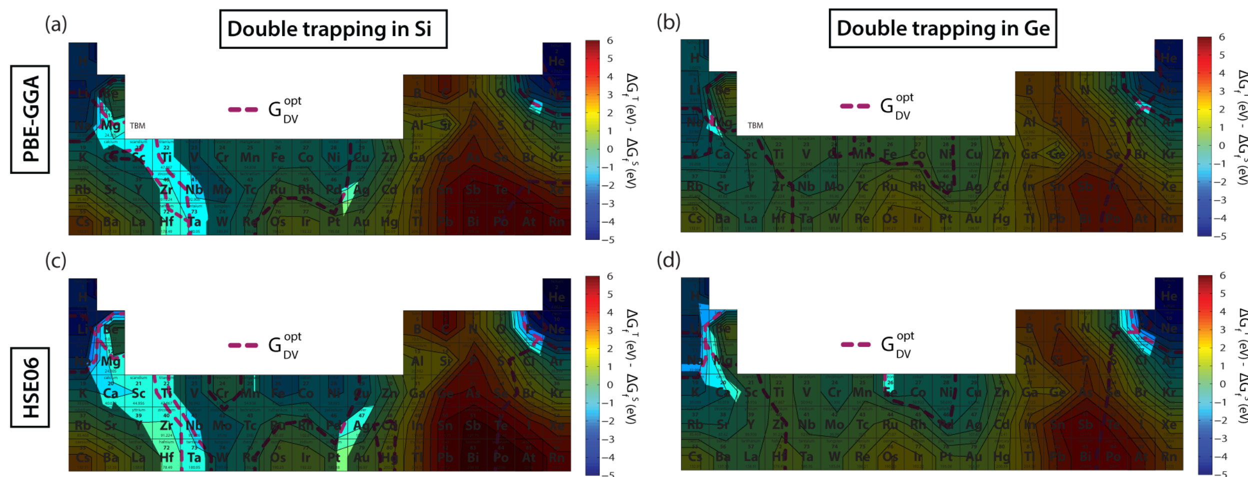

Figure 6. Optimal double-trapping regions at the melting temperature with the PBE functional for (a) Si and (b) Ge and with the HSE06 functional for (c) Si and (d) Ge. Here the contours represent $\Delta G_\mathrm{f}^\mathrm{T} - \Delta G_\mathrm{f}^\mathrm{S}$, and all areas excluded in Figure 4 have been darkened. Double trapping is most likely when the first free trap is more prevalent, i.e., where $\Delta G_\mathrm{f}^\mathrm{T} - \Delta G_\mathrm{f}^\mathrm{S}$ is negative.

formation enthalpy of the vacancy shifts both H_DV and the boundaries in the same direction, with further cancellation of enthalpic changes in the remaining terms of eq 6. In the case of Si, the cross sections for Li−Be and F remain largely identical, while in the transition metal region the cross sections shift toward Nb from Mo, including Ti, and toward Ag from Pd. The behavior for Ge is similar, with Nb and Ag also entering the double-trapping region. These results suggest that while HSE06 may cause a minor shift in the final results, it is still recommended to perform initial screening with PBE followed by local exploration of good candidates and their surroundings using HSE06. In this way computational resources can be saved during the PBE screening phase and reinvested in higher-accuracy HSE06 calculations.

Vacancy Trapping at the Melting Temperature. By the use of Gibbs free energies of formation, the trapping enthalpy H_DV can be converted to the trapping Gibbs free energy G_DV:

$$G_\mathrm{DV} = \Delta G_\mathrm{f}^\mathrm{DV} - \Delta G_\mathrm{f}^\mathrm{D} - \Delta G_\mathrm{f}^\mathrm{V} \tag{11}$$

Making use of the fact that $g_\mathrm{D} = 1$ for D = V, S, and T, this can be rewritten as

$$G_\mathrm{DV} = H_\mathrm{DV} - k_\mathrm{B}T \ln\left(\frac{W_\mathrm{DV}}{W_\mathrm{D}W_\mathrm{V}}\right) = H_\mathrm{DV} - k_\mathrm{B}T \ln(g_\mathrm{DV}C) \tag{12}$$

where $C = 1/N$ is the impurity concentration. This will cause the trapping enthalpy to increase because C is always smaller than 1. Similarly, the selection quantities can be replaced by their Gibbs free energy counterparts,

$$\Delta G_\mathrm{f}^\mathrm{D} = \Delta H_\mathrm{f}^\mathrm{D} + k_\mathrm{B}T \ln\left(\frac{C}{g_\mathrm{D}}\right) \tag{13}$$

which will decrease in value.

The same elimination procedure can now be performed at the melting temperature and a given concentration C. A typical defect concentration of 10^{15} cm^{-3} was chosen for Si, which reduces to an occupancy of 1 in 2×10^{-8} Si lattice sites. The same atomic concentration was used for Ge. This causes the following change in intervals and optimal values for PBE:

- for Si: -1.0 eV < H_DV < 0 eV; $H_\mathrm{DV}^\mathrm{opt} = -0.4$ eV; $\Delta H_\mathrm{f}^\mathrm{D}$ < 1.0 eV
- for Ge: -0.6 eV < H_DV < 0 eV; $H_\mathrm{DV}^\mathrm{opt} = -0.3$ eV; $\Delta H_\mathrm{f}^\mathrm{D}$ < 0.7 eV

The intervals and optimal values for HSE06 are:

- for Si: -1.9 eV < H_DV < 0 eV; $H_\mathrm{DV}^\mathrm{opt} = -0.5$ eV; $\Delta H_\mathrm{f}^\mathrm{D}$ < 1.9 eV
- for Ge: -1.7 eV < H_DV < 0 eV; $H_\mathrm{DV}^\mathrm{opt} = -0.5$ eV; $\Delta H_\mathrm{f}^\mathrm{D}$ < 1.7 eV

The resulting double-trapping regions are shown in Figure 6.

Compared to the 0 K results, the optimal regions have contracted but remain centered around the same areas, albeit slightly shifted. There is more correspondence between the PBE and HSE06 results, but there is again a minor shift in the region with now an expansion in both cases. This is the case because V and Cr were already excluded from the PBE candidates upon addition of the entropic contributions to the Gibbs free energies. For both Si and Ge, the Li−Mg and F−Cl regions provide the true cross sections. These regions contain monovalent impurities that may be able to passivate some of the dangling bonds. F−V complex formation has been observed experimentally.[45] Transition metal regions remain for Si but are nearly fully excluded in the case of Ge. Only Fe remains as a candidate in the HSE06 results. Because of the limited change in the enthalpy surfaces, however, the optimal transition metals at 0 K remain the best suboptimal choices in this region. For Si, Nb−Zr and Ti remain good candidates, with Sc added for PBE. One can conclude that both temperature and the contribution of HF exchange cause changes in the screening results but that these are not as large as one might expect. As a result, the PBE candidate set offers an acceptable first attempt at discovering optimal vacancy traps under the described conditions. To further improve upon the selected candidates, the optimal regions should be studied in more detail with HSE06 calculations performed with higher precision and vibrational contributions to the entropy. To obtain a more complete picture, the same procedure can also be repeated with self-interstitials. With information on both native defects in hand, their relative concentrations after Frenkel pair recombination can be estimated. This is most relevant to tune the defect

DOI: 10.1021/acs.chemmater.6b03368
Chem. Mater. 2017, 29, 975−984

concentrations in or close to regimes where the two exist simultaneously.

■ CONCLUSIONS

A database was constructed to study the behavior of 73 impurities at six positions in Si and Ge. Formation enthalpies and Gibbs free energies at the melting temperature were determined using both the PBE and HSE06 DFT functionals. From these results, the lowest-enthalpy positions were derived for each impurity and found to be in close agreement with experiment. The most notable PBE result was the occurrence of an interstitial region for the transition metals in Si that does not exist for Ge. While this was experimentally known, the current database suggests that this behavior extends toward heavier elements for the left upper triangle of the periodic table. The HSE06 functional shows largely the same behavior but imposes a higher energetic penalty on the creation of vacancies. This shifts several impurities from divacancy (BC, SV) to single-vacancy (S, TV) positions and from single-vacancy positions to interstitials (T, H). The same behavior occurs in the transition metal region for Ge, which is not observed experimentally. This difference may be a side effect of limited numerical precision but also may imply that other effects, such as charge or configurational or vibrational entropy, may serve to reverse some of the observed shifts. Temperature dependence was estimated through configurational entropy, which at the melting temperature makes a sizable contribution to the Gibbs free energy and is likely underestimated. The vibrational contribution may provide an additional non-negligible contribution but is out of scope for a high-throughput study. The configurational entropy showed that many defects obtained a partial occupancy, usually by shifting toward their asymmetrical equivalent sites (i.e., a vacancy pair rather than S or BC sites). The second part of the paper illustrated an elimination procedure that screened candidates for vacancy gettering in a Si or Ge melt. This was achieved by deriving secondary quantities from the database, and the effects of both temperature and the functional were again considered. In both cases, changes in the end result were fairly limited and several interesting areas of the periodic table were highlighted. Further research on these candidates has the potential to yield practical impurities for vacancy gettering and in this way would provide an industrially relevant quality boost of Ge wafers. While more detailed studies are surely needed, this application demonstrates how high-throughput ab initio screening is capable of not only reproducing experimental data sets but also expanding them, in this way uncovering trends that might not be visible from the limited experimental data. It was also shown that because of the size of the data set, many secondary properties are inherently present within the database. As demonstrated, these can be used to easily perform a secondary screening step that selects candidate impurities for industrially relevant applications. The entire database, including enthalpy data and many additional graphs used during the selection of candidate vacancy traps as well as defect geometries, can be found in the Supporting Information. Combining the current database with additional data sets, such as charge states, vibrational frequencies, migration barriers, or optical transition levels, would further expand the discussed possibilities. This would also enable the use of modern data-mining techniques, which can uncover complex relations and trends that go far beyond those that can be directly visually identified. These types of discoveries would never be possible experimentally because of the sheer cost, in both time and money, of growing and characterizing the single crystals representing all of these data points.

■ COMPUTATIONAL DETAILS

The database consists of two sets of calculations, both based on periodic DFT. Their main distinction is the functional used. Relaxed geometries and initial formation enthalpies were obtained using the Perdew−Burke−Ernzerhof (PBE) functional.[31,32] These relaxed geometries were then used to perform additional calculations with the 2006 Heyd−Scuseria−Ernzerhof (HSE06) hybrid functional, a modification of PBE in which a short-range correction of the exchange interaction using exact exchange from a Hartree−Fock calculation is applied.[33] These calculations were performed sequentially using in-house automation software Queue Manager, which interfaces with various popular DFT packages.[46]

The starting geometry of the PBE calculations was a direct result of the choice of the model system. In the case of semiconductor defects, it was defined by the size of the host supercell. This was chosen such that the concentration of defects was sufficiently low to minimize the interaction between periodic copies of the defects. The host cell was chosen to contain 64 atoms, each of which was allowed to relax to its minimum-enthalpy position. Tests for a 216-atom cell suggested a 1% deviation in ΔH_f, which did not affect the trends of interest in this work. The following paragraphs will discuss the details of the PBE and HSE06 calculations.

The PBE calculations were performed using the all-electron linearized augmented plane wave (LAPW) method as implemented in the WIEN2k 12.1 software package.[47,48] While PBE strongly underestimates the band gap for both materials, it is computationally relatively cheap and provides accurate formation enthalpies.[37,49] The numerical precision of the formation enthalpies ΔH_f was calibrated to a total error below 0.01 eV per defect cell. Settings for the lower-symmetry vacancy complexes were adapted to reach an equivalent precision level. The reciprocal grid for defect cells was chosen to contain at least 20 **k** points during relaxation for point defects and 40 **k** points for vacancy complexes. Final energy calculations were performed with a minimal mesh of 50 and 100 **k** points for point defects and complexes, respectively. The grid density was automatically raised when convergence issues occurred. Final energies for impurity reference states were calculated using a minimal **k** mesh of $8000/N_{at}$ **k** points, where N_{at} is the number of atoms. Si and Ge host cells were calculated using 64-atom supercells with identical settings as the defect calculations to maximize cancellation of errors. Reference geometries were not relaxed since these were previously optimized with the same functional using the Vienna Ab Initio Software Package (VASP).[3] The basis set size is determined by the K_{max} parameter, which was kept constant at 3.10 for relaxations and 3.57 for final energy calculations. To ensure sufficient precision, K_{max} was further increased to 5.00 for H defects. The input parameter that determines K_{max} is called RK_{max} in WIEN2k. It is always set equal to $R_{mt,min} \cdot K_{max}$, the product of the minimal muffin-tin sphere radius present in the cell and the desired K_{max}. Spin polarization was enabled for known magnetic impurities (Cr, Mn, Fe, Co, and Ni). Spin−orbit coupling was enabled for heavy impurities starting at Cs. In most cases, R_{mt} was chosen as 1.9 bohr for Si and 2.0 bohr for Ge, with separate reference states for each. On the basis of the R_{mt} recommended for impurities by WIEN2k's `init_lapw`, fixed R_{mt} values of 2.02 and 2.13 bohr were chosen for impurities in Si and Ge, respectively. The R_{mt} values of period 1 and 2 elements required manual adaptation because of their small radii. Full details concerning the purpose and implementation of these settings can be found in the WIEN2k manual.[47]

The HSE06 calculations were performed in VASP 5.3 using the projector-augmented wave (PAW) method.[50−54] This method does not require explicit calculation of the core electrons, greatly reducing the required computational time. This is essential because calculating the HF contribution for even a single **k** point can lead to a 100-fold increase in the total calculation time. Therefore, only a static energy calculation based on the PBE geometry was performed, with no additional relaxation of the defect cell. Calculating the HF exchange on

DOI: 10.1021/acs.chemmater.6b03368
Chem. Mater. 2017, 29, 975−984

a reduced **k** mesh inevitably lowers the numerical precision to some extent. Even with this limitation, the HSE06 functional is able to significantly alter the formation enthalpy as well as correct the band gaps of both the Si and Ge host materials. This is significant, especially for Ge, which has a metallic band structure at the PBE level.[34,35] The variation of the PBE formation enthalpies throughout the data set is fairly large (5−10 eV) and is further spread out by the hybrid functional. This means that the reduced numerical precision in the HSE06 case does little to change the trends but can make it difficult to distinguish between defect sites of similar energy. The PBE contribution was still calculated on a larger grid consisting of 6 × 6 × 6 **k** points (20−32 irreducible) for Si and 4 × 4 × 4 **k** points (10−13 irreducible) for Ge because of the increased computational intensity resulting from the inclusion of d electrons. Within VASP a plane-wave basis set is used, the size of which is determined by the cutoff energy E_{cut}. It was set to 600 eV for impurities from the first two rows of the periodic table and 400 eV for those from lower rows. The real-space grid was kept sufficiently dense for all calculations using `PREC = Accurate`, while `PRECFOCK` was kept at `Normal`. Spin-polarization was considered for the same elements as in the PBE calculations. Spin−orbit coupling was not considered, as its effect is small and its computation is not feasible in combination with HSE06. Reference states were relaxed using HSE06, though not to the same accuracy as for the PBE reference set, which contributes to the larger error bar mentioned previously. Fully optimized geometries will be published at a later date. Energies were calculated with an E_{cut} matching that of the defect cells and a 12 × 12 × 12 PBE **k** mesh, which was reduced to 6 × 6 × 6 for the HF contribution, making the numerical error for the reference states negligible.

ASSOCIATED CONTENT

Supporting Information

The Supporting Information is available free of charge on the ACS Publications website at DOI: 10.1021/acs.chemmater.6b03368.

Relaxed geometries in CIF format for all of the studied impurities and positions (ZIP)

Database of formation enthalpies and additional vacancy trapping figures not included in the main article (PDF)

AUTHOR INFORMATION

Corresponding Authors

*E-mail: michael.sluydts@ugent.be.

*E-mail: stefaan.cottenier@ugent.be.

ORCID

Michael Sluydts: 0000-0003-2798-3257

Present Address

‖M.P.: Department of Information and Communication Technology, Vrije Universiteit Brussel (VUB), 1050 Brussels, Belgium.

Notes

The authors declare no competing financial interest.

ACKNOWLEDGMENTS

This work was supported by the Fund for Scientific Research—Flanders (FWO) (Project G.0760.12) and the Research Board of Ghent University. The computational resources and services used in this work were provided by the VSC (Flemish Supercomputer Center), funded by the Hercules Foundation and the Flemish Government—Department EWI. S.C. acknowledges financial support from OCAS NV by an OCAS-endowed chair at Ghent University. S.C. acknowledges stimulating discussions with A. Vantomme and S. Decoster in an early phase of this work. All of the authors are indebted to Jan Vanhellemont, a coauthor of this paper, who passed away while this article was being written. His enthusiasm and vast semiconductor knowledge will be missed. An overview of his career can be found in ref 15.

REFERENCES

(1) Curtarolo, S.; Hart, G. L. W.; Nardelli, M. B.; Mingo, N.; Sanvito, S.; Levy, O. The High-Throughput Highway to Computational Materials Design. *Nat. Mater.* **2013**, *12*, 191−201.

(2) Lejaeghere, K.; et al. Reproducibility in Density Functional Theory Calculations of Solids. *Science (Washington, DC, U. S.)* **2016**, *351*, aad3000.

(3) Lejaeghere, K.; Van Speybroeck, V.; Van Oost, G.; Cottenier, S. Error Estimates for Solid-State Density-Functional Theory Predictions: an Overview by Means of the Ground-State Elemental Crystals. *Crit. Rev. Solid State Mater. Sci.* **2014**, *39*, 1−24.

(4) Kirklin, S.; Saal, J. E.; Meredig, B.; Thompson, A.; Doak, J. W.; Aykol, M.; Rühl, S.; Wolverton, C. The Open Quantum Materials Database (OQMD): Assessing the Accuracy of DFT Formation Energies. *npj Comput. Mater.* **2015**, *1*, 15010.

(5) Castelli, I. E.; Olsen, T.; Datta, S.; Landis, D. D.; Dahl, S.; Thygesen, K. S.; Jacobsen, K. W. Computational Screening of Perovskite Metal Oxides for Optimal Solar Light Capture. *Energy Environ. Sci.* **2012**, *5*, 5814−5819.

(6) Liu, M.; Rong, Z.; Malik, R.; Canepa, P.; Jain, A.; Ceder, G.; Persson, K. A. Spinel Compounds as Multivalent Battery Cathodes: a Systematic Evaluation Based on Ab Initio Calculations. *Energy Environ. Sci.* **2015**, *8*, 964−974.

(7) Bhattacharya, S.; Madsen, G. K. H. High-Throughput Exploration of Alloying as Design Strategy for Thermoelectrics. *Phys. Rev. B: Condens. Matter Mater. Phys.* **2015**, *92*, 085205.

(8) Armiento, R.; Kozinsky, B.; Hautier, G.; Fornari, M.; Ceder, G. High-throughput Screening of Perovskite Alloys for Piezoelectric Performance and Thermodynamic Stability. *Phys. Rev. B: Condens. Matter Mater. Phys.* **2014**, *89*, 134103.

(9) Greeley, J.; Jaramillo, T. F.; Bonde, J.; Chorkendorff, I. B.; Nørskov, J. K. Computational High-Throughput Screening of Electrocatalytic Materials for Hydrogen Evolution. *Nat. Mater.* **2006**, *5*, 909−913.

(10) Wilmer, C. E.; Leaf, M.; Lee, C. Y.; Farha, O. K.; Hauser, B. G.; Hupp, J. T.; Snurr, R. Q. Large-scale Screening of Hypothetical Metal-Organic Frameworks. *Nat. Chem.* **2011**, *4*, 83−89.

(11) Kolmogorov, A. N.; Calandra, M.; Curtarolo, S. Thermodynamic Stabilities of Ternary Metal Borides: an Ab Initio Guide for Synthesizing Layered Superconductors. *Phys. Rev. B: Condens. Matter Mater. Phys.* **2008**, *78*, 094520.

(12) *Germanium-Based Technologies*, 1st ed.; Claeys, C., Simoen, E., Eds.; Elsevier: Oxford, U.K., 2007; Chapters 1 and 2.

(13) Brinkman, W.; Haggan, D.; Troutman, W. A History of the Invention of the Transistor and Where it Will Lead Us. *IEEE J. Solid-State Circuits* **1997**, *32*, 1858−1865.

(14) Riordan, M. The Lost History of the Transistor. *IEEE Spectrum* **2004**, *41*, 44−49.

(15) Kissinger, G.; Simoen, E.; Claeys, C.; Clauws, P.; Śpiewak, P.; Sueoka, K.; Yang, D. Jan Vanhellemont − 35 Years of Materials Research in Microelectronics. *Phys. Status Solidi C* **2016**, *13*, 706−711.

(16) Madelung, O. *Semiconductors: Data Handbook*; Springer: Berlin, 2013; Chapter 1.

(17) *Impurities and Defects in Group IV Elements, IV−IV and III−V Compounds. Part a: Group IV Elements*; Madelung, O., Rössler, U., Schulz, M., Eds.; Landolt-Börnstein - Group III Condensed Matter, Vol. *41A2a*; Springer: Berlin, 2002; Chapters 132, 152, 162, and 164.

(18) Maeta, T.; Sueoka, K. Density Functional Theory Calculations of Stability and Diffusion Mechanisms of Impurity Atoms in Ge Crystals. *J. Appl. Phys. (Melville, NY, U. S.)* **2014**, *116*, 073505.

(19) Artacho, E.; Ynduráin, F.; Pajot, B.; Ramírez, R.; Herrero, C. P.; Khirunenko, L. I.; Itoh, K. M.; Haller, E. E. Interstitial Oxygen in Germanium and Silicon. *Phys. Rev. B: Condens. Matter Mater. Phys.* **1997**, *56*, 3820−3833.

(20) Decoster, S.; Cottenier, S.; De Vries, B.; Emmerich, H.; Wahl, U.; Correia, J. G.; Vantomme, A. Transition Metal Impurities on the Bond-Centered Site in Germanium. *Phys. Rev. Lett.* **2009**, *102*, 065502.
(21) Decoster, S.; Cottenier, S.; Wahl, U.; Correia, J. G.; Pereira, L. M. C.; Lacasta, C.; Da Silva, M. R.; Vantomme, A. Diluted Manganese on the Bond-centered Site in Germanium. *Appl. Phys. Lett.* **2010**, *97*, 151914.
(22) Decoster, S.; Cottenier, S.; Wahl, U.; Correia, J. G.; Vantomme, A. Lattice Location Study of Ion Implanted Sn and Sn-related Defects in Ge. *Phys. Rev. B: Condens. Matter Mater. Phys.* **2010**, *81*, 155204.
(23) Decoster, S.; Wahl, U.; Cottenier, S.; Correia, J. G.; Mendonça, T.; Amorim, L. M.; Pereira, L. M. C.; Vantomme, A. Lattice Position and Thermal Stability of Diluted As in Ge. *J. Appl. Phys. (Melville, NY, U. S.)* **2012**, *111*, 053528.
(24) Sueoka, K.; Kamiyama, E.; Spiewak, P.; Vanhellemont, J. Review—Properties of Intrinsic Point Defects in Si and Ge Assessed by Density Functional Theory. *ECS J. Solid State Sci. Technol.* **2016**, *5*, P3176−P3195.
(25) Chroneos, A.; Bracht, H.; Grimes, R. W.; Uberuaga, B. P. Vacancy-mediated dopant diffusion activation enthalpies for germanium. *Appl. Phys. Lett.* **2008**, *92*, 172103.
(26) Kube, R.; Bracht, H.; Chroneos, A.; Posselt, M.; Schmidt, B. Intrinsic and extrinsic diffusion of indium in germanium. *J. Appl. Phys. (Melville, NY, U. S.)* **2009**, *106*, 063534.
(27) Tahini, H.; Chroneos, A.; Grimes, R. W.; Schwingenschlögl, U.; Bracht, H. Diffusion of E centers in germanium predicted using GGA+U approach. *Appl. Phys. Lett.* **2011**, *99*, 072112.
(28) Chroneos, A.; Bracht, H. Diffusion of n-type dopants in germanium. *Appl. Phys. Rev.* **2014**, *1*, 011301.
(29) Tahini, H. A.; Chroneos, A.; Middleburgh, S. C.; Schwingenschlögl, U.; Grimes, R. W. Ultrafast palladium diffusion in germanium. *J. Mater. Chem. A* **2015**, *3*, 3832−3838.
(30) Kujala, J.; Südkamp, T.; Slotte, J.; Makkonen, I.; Tuomisto, F.; Bracht, H. Vacancy-donor complexes in highly n-type Ge doped with As, P and Sb. *J. Phys.: Condens. Matter* **2016**, *28*, 335801.
(31) Perdew, J. P.; Burke, K.; Ernzerhof, M. Generalized Gradient Approximation Made Simple. *Phys. Rev. Lett.* **1996**, *77*, 3865−3868.
(32) Perdew, J. P.; Burke, K.; Ernzerhof, M. Erratum: Generalized Gradient Approximation Made Simple. *Phys. Rev. Lett.* **1997**, *78*, 1396.
(33) Krukau, A. V.; Vydrov, O. A.; Izmaylov, A. F.; Scuseria, G. E. Influence of the Exchange Screening Parameter on the Performance of Screened Hybrid Functionals. *J. Chem. Phys.* **2006**, *125*, 224106.
(34) Śpiewak, P.; Kurzydłowski, K. J. Formation and Migration Energies of the Vacancy in Si Calculated Using the HSE06 Range-separated Hybrid Functional. *Phys. Rev. B: Condens. Matter Mater. Phys.* **2013**, *88*, 195204.
(35) Śpiewak, P.; Vanhellemont, J.; Kurzydłowski, K. J. Improved Calculation of Vacancy Properties in Ge using the Heyd-Scuseria-Ernzerhof Range-separated Hybrid Functional. *J. Appl. Phys. (Melville, NY, U. S.)* **2011**, *110*, 063534.
(36) Hummer, K.; Harl, J.; Kresse, G. Heyd-Scuseria-Ernzerhof hybrid functional for calculating the lattice dynamics of semiconductors. *Phys. Rev. B: Condens. Matter Mater. Phys.* **2009**, *80*, 115205.
(37) Freysoldt, C.; Grabowski, B.; Hickel, T.; Neugebauer, J.; Kresse, G.; Janotti, A.; Van de Walle, C. G. First-principles Calculations for Point Defects in Solids. *Rev. Mod. Phys.* **2014**, *86*, 253−305.
(38) Sawada, H.; Kawakami, K. First-principles Calculation of the Interaction Between Nitrogen Atoms and Vacancies in Silicon. *Phys. Rev. B: Condens. Matter Mater. Phys.* **2000**, *62*, 1851−1858.
(39) Kapur, S. S.; Prasad, M.; Crocker, J. C.; Sinno, T. Role of configurational entropy in the thermodynamics of clusters of point defects in crystalline solids. *Phys. Rev. B: Condens. Matter Mater. Phys.* **2005**, *72*, 014119.
(40) Vanhellemont, J.; Kamiyama, E.; Sueoka, K. Silicon Single Crystal Growth from a Melt: On the Impact of Dopants on the v/G Criterion. *ECS J. Solid State Sci. Technol.* **2013**, *2*, P166−P179.
(41) Voronkov, V.; Falster, R. The Diffusivity of the Vacancy in Silicon: Is it Fast or Slow? *Mater. Sci. Semicond. Process.* **2012**, *15*, 697−702.
(42) Kamiyama, E.; Sueoka, K.; Vanhellemont, J. Formation Energy of Intrinsic Point Defects in Si and Ge and Implications for Ge Crystal Growth. *ECS J. Solid State Sci. Technol.* **2013**, *2*, P104−P109.
(43) Lejaeghere, K.; Cottenier, S.; Van Speybroeck, V. Ranking the Stars: A Refined Pareto Approach to Computational Materials Design. *Phys. Rev. Lett.* **2013**, *111*, 075501.
(44) Voronkov, V.; Falster, R. Nitrogen Interaction with Vacancies in Silicon. *Mater. Sci. Eng., B* **2004**, *114*−*115*, 130−134.
(45) Simpson, P. J.; Jenei, Z.; Asoka-Kumar, P.; Robison, R. R.; Law, M. E. Observation of Fluorine-Vacancy Complexes in Silicon. *Appl. Phys. Lett.* **2004**, *85*, 1538−1540.
(46) The current repository for this software package can be found at https://github.com/MichaelSluydts/QueueManager.
(47) Blaha, P.; Schwarz, K.; Madsen, G.; Kvasnicka, D.; Luitz, J. *WIEN2k: An Augmented Plane Wave Plus Local Orbitals Program for Calculating Crystal Properties*; Vienna University of Technology: Vienna, Austria, 2013.
(48) Cottenier, S. *Density Functional Theory and the Family of (L)APW-Methods: A Step-by-Step Introduction*; Instituut voor Kern- en Stralingsfysica, K.U. Leuven: Heverlee, Belgium, 2002; freely available at http://www.wien2k.at/reg_user/textbooks.
(49) Lejaeghere, K.; Cottenier, S.; Claessens, S.; Waroquier, M.; Van Speybroeck, V. Assessment of a Low-Cost Protocol for an Ab Initio Based Prediction of the Mixing Enthalpy at Elevated Temperatures: The Fe-Mo System. *Phys. Rev. B: Condens. Matter Mater. Phys.* **2011**, *83*, 184201.
(50) Kresse, G.; Hafner, J. Ab Initio Molecular Dynamics for Liquid Metals. *Phys. Rev. B: Condens. Matter Mater. Phys.* **1993**, *47*, 558−561.
(51) Kresse, G.; Hafner, J. Ab initio Molecular-Dynamics Simulation of the Liquid-Metal-Amorphous-Semiconductor Transition in Germanium. *Phys. Rev. B: Condens. Matter Mater. Phys.* **1994**, *49*, 14251−14269.
(52) Kresse, G.; Furthmüller, J. Efficiency of Ab-Initio Total Energy Calculations for Metals and Semiconductors Using a Plane-Wave Basis Set. *Comput. Mater. Sci.* **1996**, *6*, 15−50.
(53) Kresse, G.; Furthmüller, J. Efficient Iterative Schemes for Ab Initio Total-Energy Calculations Using a Plane-Wave Basis Set. *Phys. Rev. B: Condens. Matter Mater. Phys.* **1996**, *54*, 11169−11186.
(54) Kresse, G.; Joubert, D. From Ultrasoft Pseudopotentials to the Projector Augmented-Wave Method. *Phys. Rev. B: Condens. Matter Mater. Phys.* **1999**, *59*, 1758−1775.

DOI: 10.1021/acs.chemmater.6b03368
Chem. Mater. 2017, 29, 975−984